

Glioblastoma initiating cells are sensitive to histone demethylase inhibition due to epigenetic deregulation

Jan-Philipp Mallm¹, Paul Windisch², Alva Biran³, Zoltan Gal⁴, Sabrina Schumacher¹, Rainer Glass⁵, Christel Herold-Mende⁴, Eran Meshorer³, Martje Barbus² and Karsten Rippe¹ 

¹Division of Chromatin Networks, German Cancer Research Center (DKFZ), Heidelberg, Germany

²Division of Molecular Genetics, German Cancer Research Center (DKFZ), Heidelberg, Germany

³Department of Genetics, Institute of Life Sciences, and the Edmond and Lily Safra Center for Brain Sciences (ELSC), The Hebrew University of Jerusalem, Jerusalem, Israel

⁴Division of Neurosurgical Research, Department of Neurosurgery, University of Heidelberg, Heidelberg, Germany

⁵Neurosurgical Research, University Hospital, LMU Munich, Munich, Germany

Tumor-initiating cells are a subpopulation of cells that have self-renewal capacity to regenerate a tumor. Here, we identify stem cell-like chromatin features in human glioblastoma initiating cells (GICs) and link them to a loss of the repressive histone H3 lysine 9 trimethylation (H3K9me3) mark. Increasing H3K9me3 levels by histone demethylase inhibition led to cell death in GICs but not in their differentiated counterparts. The induction of apoptosis was accompanied by a loss of the activating H3 lysine 9 acetylation (H3K9ac) modification and accumulation of DNA damage and downregulation of DNA damage response genes. Upon knockdown of histone demethylases, KDM4C and KDM7A both differentiation and DNA damage were induced. Thus, the H3K9me3–H3K9ac equilibrium is crucial for GIC viability and represents a chromatin feature that can be exploited to specifically target this tumor subpopulation.

Introduction

Glioblastoma multiforme (GBM) is an aggressive brain tumor with a mean survival rate of less than 1 year.¹ Glioblastoma initiating cells (GICs) represent a small subpopulation of cells in this tumor with stem cell characteristics. They can continuously self-renew and regenerate the tumor.^{2–4} GICs are resistant against radiation and chemotherapy *in vitro* and *in vivo*, probably due to

an increased efficiency to repair DNA damage and a slow mitotic turnover.^{5–8} Accordingly, tumor recurrences after treatment of GBM have been linked to the regeneration of tumor cells from GICs.^{7,9} These considerations underline the need for identifying deregulated pathways that could be exploited to specifically target GICs or induce their differentiation and subsequent tumor shrinkage. Here, we investigated chromatin features associated with the

Alva Biran's current address is: Biotech Research and Innovation Centre (BRIC) and Novo Nordisk Center for Protein Research (CPR), Faculty of Health and Medical Sciences, University of Copenhagen, Copenhagen, Denmark

Additional Supporting Information may be found in the online version of this article.

Key words: cancer stem cells, histone methylation, histone acetylation, heterochromatin, DNA repair

Abbreviations: ESCs: embryonic stem cells; FRAP: fluorescence recovery after photobleaching; GBM: glioblastoma multiforme; GFP: green fluorescent protein; GIC: glioblastoma initiating cell; H3K9me3: histone H3 lysine 9 trimethylation; HP1: heterochromatin protein 1; IF: immunofluorescence; JMJ: jumonji; NPC: neuronal precursor cell; SUV39H1: suppressor of variegation 3–9 homolog 1

Conflict of Interest: The authors declare no conflict of interest.

Grant sponsor: Cooperation program between the DKFZ and Israel's Ministry of Science, Technology and Space; **Grant numbers:** Ca146, Ca180; **Grant sponsor:** Deutsche Forschungsgemeinschaft; **Grant number:** German CellNetworks Cluster of Excellence (EXC81)

This is an open access article under the terms of the Creative Commons Attribution-NonCommercial-NoDerivs License, which permits use and distribution in any medium, provided the original work is properly cited, the use is non-commercial and no modifications or adaptations are made.

DOI: 10.1002/ijc.32649

History: Received 7 Mar 2019; Accepted 30 Jul 2019; Online 28 Aug 2019

Correspondence to: Jan-Philipp Mallm, Division of Chromatin Networks, German Cancer Research Center (DKFZ), Heidelberg, Germany, E-mail: j.mallm@dkfz.de; or Karsten Rippe, Division of Chromatin Networks, German Cancer Research Center (DKFZ), Heidelberg, Germany, E-mail: karsten.rippe@dkfz.de

What's new?

Glioblastoma-initiating cells (GICs) exhibit stem cell-like properties, including the capacity for continuous self-renewal. In this study, owing to the relevance of histone methylation and acetylation to DNA repair and self-renewal in mouse and human embryonic stem cells, the authors investigated chromatin features in GICs. Analyses show that GICs possess an open chromatin structure, with enrichment of histone acetylation and reduced methylation. Inhibition of the histone demethylases KDM4C and KDM7A, leading to global restoration of H3K9me3 levels, reduced viability and induced differentiation in GICs. The findings suggest that selective targeting of histone demethylases is a promising strategy for eliminating GIC subpopulations.

stem cell-like state of GICs. It was shown previously that an increased plastic and open chromatin state was linked to pluripotency and the self-renewal potential of mouse and human embryonic stem cells (mESCs/hESCs).^{10,11} The chromatin distribution in the nucleus of these stem cells was more homogeneous and chromosomal proteins displayed an increased mobility than the corresponding differentiated cells. In addition, specific patterns of epigenetic modifications were observed that include a global decrease of histone H3 lysine 9 trimethylation (H3K9me3)^{12–15} while H3K9 acetylation, a signature of open chromatin, was increased in human ESCs.¹⁶ Thus, the balance between histone methylation and acetylation of H3K9 is shifted toward the acetylated state in stem cells. This conclusion is supported by the finding that H3K9me3 inhibits somatic cell reprogramming into induced pluripotent stem cells^{17,18} while histone deacetylation inhibitors enhance reprogramming of somatic cells into induced pluripotent cells.¹⁹ Likewise, knockdown of the KDM4C (JMJD2C) and KDM3A (JMJD1A) histone demethylases of histone H3 trimethylated at lysine 9 (H3K9me3) resulted in differentiation of ESCs.²⁰ Furthermore, an open chromatin structure has been associated with a high DNA repair capacity,^{21–23} whereas H3K9me3 was reported to counteract ATM activation.^{24,25} Finally, we recently showed that, similar to pluripotent cells, cancer stem cells show reduced levels of the linker histone variant H1.0 leading to a more dynamic chromatin organization.²⁶

The above findings led us to test the following hypothesis in the present study: the balance between eu- and heterochromatin and associated histone modifications in GICs shares similarities with stem cell chromatin. This aberrant chromatin state is functionally important for their ability to maintain their proliferation potential, genome stability and full DNA repair capacity. We report that GICs, akin to ESCs, displayed an open and highly dynamic chromatin structure with loss of clustered H3K9me3. At the same time, H3K9 showed aberrant hyperacetylation at promoters linked to a deregulated DNA damage response (DDR). By inhibition of histone demethylases, we validated our model for the underlying mechanism and demonstrate that the selective targeting of KDM4C and KDM7A induces apoptosis and differentiation in GICs.

Materials and Methods**Cell culture and transient transfections**

Mouse 129/Ola ESCs²⁷ used for this study were cultured in serum-free PowerStem ESPro1 (PAN, Aidenbach, Germany). The medium was supplemented with human leukemia inhibitory

factor (hLIF) produced in HEK cells. Differentiation of ESCs into neuronal precursors was induced *via* formation of embryoid bodies in FCS containing STEMPAN medium (PAN) for 4 days. After treatment with 5 μ M retinoic acid, neuronal embryoid bodies were dissociated and seeded on matrigel in neuronal stem cell medium (PAN) for 2 days. The NCH421k (CVCL_X910), NCH644 (CVCL_X914) and NCH441 (RRID:CVCL_X912) cell lines were derived from glioblastoma samples and have been described previously.^{28–30} Cells were cultured as neuronal spheres in neuronal base medium supplemented with BIT9500 (Provitro, Berlin, Germany), basic fibroblast growth factor (bFGF, Provitro) and epidermal growth factor (EGF, Biomol, Hamburg, Germany) at 20 ng/ μ l. For differentiation, GICs were seeded on adherent surfaces in DMEM with 10% FCS, glutamine and 500 nM retinoic acid (Biomol) for up to 3 weeks. Plasmids transfection was conducted with lipofectamine 2000 (ThermoFisher Scientific, Dreieich, Germany) at 1.5 (ESCs) and 2 (GICs) times higher amounts than recommended by the manufacturer. A summary of the different cell line samples is given in Supplementary - Table S2. All cell lines were tested for the absence of mycoplasma with the VenorGeM Advance kit (Minerva Biolabs, Berlin, Germany), and human cell lines were authenticated using single nucleotide polymorphism-profiling (Multiplexion).

Cultivated subventricular neural precursor cells from adult human SVZ specimens (SVZ-NPC) were generated as part of planned resections in patients during anterior temporal lobectomy for the treatment of intractable epilepsy from mesial temporal sclerosis. Ethical approval was obtained (UE-Nr.: 122-13). Tissue was mechanically minced and subsequently enzymatically dissociated in 1.33 mg/ml trypsin in HBSS with 2 mM glucose at 37°C for 30 min. The cells were centrifuged at 200g for 5 min, resuspended in neurobasal medium (Minerva Biolabs) supplemented with 1% HEPES, 1% L-glutamine, 1% penicillin/streptomycin, 2% B27, 20 ng/ml each of human recombinant EGF (PeproTech, Rocky Hill, NJ) and bFGF (PeproTech) and grown as neurospheres in uncoated flasks. Under these conditions, cells expanded while abundantly expressing nestin as well as PSA-NCAM, Dlx2 and doublecortin. Differentiation was induced by cultivation on laminin ornithin-coated cell-culture dishes, withdrawal of growth factors and addition of bovine serum for 14 days. It was accompanied by morphology changes and expression of β -III-tubulin, NG2, GFAP and S-100 β .

For global inhibition of jumonji (JM) family histone demethylases dimethylloxaloylglycine (DMOG) from Axxora

(Lörrach, Germany) was used. Stock solutions were prepared in DMSO and cells were treated with DMOG at a concentration of 2.5 mM in the medium for the indicated time periods. For control samples, the corresponding volume of DMSO solvent was added.

Cloning of plasmid and lentiviral vectors

The mouse plasmid constructs used for transfections have been described previously.³¹ Human *HP1* and suppressor of variegation 3–9 homolog 1 (*SUV39H1*) were cloned into pEGFP-C1 *via* Xho I and BamH I. *KDM4C* was cloned into pEGFP-N1 *via* XhoI and KpnI. To establish inducible shRNA-expressing lentiviral constructs, double-stranded oligonucleotides encoding the desired shRNAs against *KDM4A*, *KDM4B*, *KDM4C* and *KDM7A* RNAs were cloned into the single vector-inducible shRNA construct pLKO-Tet-On using the Age I and *EcoR* I restriction sites. After mixing the reconstituted sense and antisense oligonucleotides with 10× oligonucleotide annealing buffer (ThermoFisher Scientific), they were heated to 95°C for 4 min and then annealed overnight in the turned off heat block. The Roche rapid ligation kit was subsequently used to clone the resulting double-stranded oligonucleotides (0.1 nmol/μl) into the predigested and purified pLKO-Tet-On vector. The sequences of the sense and antisense oligonucleotides are listed in Supplementary Table S4. Nontarget shRNA (Mission SHC002, Nt-shRNA) served as control.

Virus production and transduction

Lentiviral particles were produced by co-transfection of HEK293T cells with the pLKO.1 shRNA constructs or inducible pLKO-Tet-On shRNA constructs and the packaging plasmids (psPAX2, pMD2.G) using TransIT-LT1 transfection reagent (Mirus Bio LLC, Madison, WI). Virus-containing supernatant was harvested 72 hr after transfection and viral particles were concentrated by ultracentrifugation. The titer was determined by FACS analysis using the pLKO.1-TurboGFP plasmid. Lentiviral transduction of the NCH644 cell line was carried out at a multiplicity of infection of 5 leading to a transduction efficiency of at least 90%. A suspension of 200,000 cells in 1 ml was transduced and distributed to 96-well plates for subsequent functional analyses. Quantification of knockdown was assessed by qRT-PCR. In order to create inducible cell lines NCH644 was infected with pLKO-Tet-On nontarget shRNA and pLKO-Tet-On shRNA lentiviral particles targeting the respective KDM. After selecting the cells with puromycin (1 μg/ml) for 7 days, they were induced in medium containing 2 μg/ml doxycycline for at least 6 days.

In vivo tumorigenicity

All animal experiments were performed according to the German animal protection law. Institutional guidelines for animal welfare and experimental conduct were followed. Either 10⁴ or

10⁶ tumor cells were implanted stereotactically into the right hemispheres of NOD/SCID mice (Charles River, Sulzfeld, Germany). Weight, general and neurological appearance of the animals were monitored frequently. Short-term monitored groups were sacrificed after 8 weeks. Long-term monitored animals were sacrificed at the onset of first general order neurological symptoms and brains were analyzed for tumor burden.

Fluorescence microscopy and immunostaining

Fluorescence microscopy was conducted using a Leica TCS SP5 confocal laser-scanning microscope equipped with a 63/1.4 numerical aperture oil-immersion objective lens (Leica Microsystems CMS). For immunofluorescence (IF), cells were seeded on matrigel coated coverslips, fixed with 4% PFA and permeabilized with 0.25% triton in PBS. Coverslips were then incubated with primary antibodies for HP1α (1:300, 2HP-1H5 Euromedex, Souffelweyersheim, France), H3K9me3 (1:300, 07-442 Millipore, Darmstadt, Germany), γH2A.X (1:100, 07-164 Millipore) and p-ATM (1:100, MAB3806 Millipore). Z-stack images were acquired and analyzed using ImageJ. For fluorescence recovery after photobleaching (FRAP) experiments, cells were seeded on matrigel coated labtek chambers transfected and then incubated for 24 hr. For each sample, at least 30 individual cells were measured with a time resolution of 270 ms/frame and an image size of 256 × 256 pixels. A circle of 1.5 μm in diameter was bleached to measure mobility in heterochromatin in ESCs, whereas a 2.5 μm circle was used for the GICs. Recovery curves were calculated and evaluated as described previously.³¹

Western blot analysis

For western blotting, 30 μg nuclear extract were loaded per lane and the following primary antibodies were used: H3K9me3 (1:300, 07-442, Millipore), H3K27me3 (1:1000, ab39155, Abcam, Cambridge, UK), H3K9ac (1:1000, 39137, Active Motif), γH2A.X (1:1000, 07-164 Millipore), H3 (1:1000, ab1791, Abcam), KDM4C (1:100, A300-885A, Bethyl Laboratories, Montgomery, TX), KDM7A (1:100, PA5-25040, ThermoFisher Scientific), β-actin (1:1000, ab8226, Abcam) and GAPDH (1:2000, AM4300 Ambion, Dreieich, Germany). Primary antibodies were detected with Alexa488-coupled secondary antibodies and signals were detected using the ChemiDoc System by Bio-Rad (Feldkirchen, Germany). Intensities were analyzed using ImageJ.

RNA-seq and ChIP-seq

Total RNA was prepared from GICs and differentiated GICs and treated with DNase I. After depletion of ribosomal RNA with Ribozero (Epicentre) and fragmentation (RNA fragmentation kit, Illumina, San Diego, CA), the RNA fragments were reverse transcribed into double stranded cDNA and subsequently cloned into an Illumina multiplex library. Single-end reads of 50 bp length were mapped to the reference genome and differential expression analysis was done with DESeq2.

ChIP-seq was performed as described in Molitor *et al.*³⁶ Single-end reads of 50 bp length were obtained, mapped with bowtie and enrichment sites were identified with MACS. Unique peaks for either GICs or differentiated cells were identified with bedtools. For GO analysis unique peaks at the promoter were identified and subjected to DAVID. For enhancer analysis, the overlap of H3K4me1 and H3K27ac was used and unique enhancers were extracted with bedtools. GREAT was used for GO analysis of unique enhancer regions using all enhancers per cell type as a background control.

RNA isolation and qRT-PCR

Total RNA was extracted using the RNeasy Mini Kit (Qiagen, Hilden, Germany) according to the manufacturer's instructions. An amount of 500 ng of total RNA was reverse transcribed using random primers and superscript II (ThermoFisher Scientific) according to the manufacturer's instructions. Each cDNA sample was analyzed in triplicate with an Applied Biosystems Prism 7900HT real-time PCR system using the Absolute SYBR Green ROX Mix (Abgene, Portsmouth, NH). The relative amount of target gene mRNA was normalized to *ARF1*, *DCTN2* and *HPRT* mRNA. Primer sequences are listed in Supplementary Table S5.

Cell viability, apoptosis and comet assays

The cell viability assay was performed in nontreated, white-walled flat bottom 96-well plates using the Celltiter-Glo Assay (Abgene). A single cell suspension of 100 μ l containing 10,000 GICs was added to each well. Each plate contained three wells per shRNA construct, at least three wells with untreated cells and three wells of medium for background measurement. On Day 5, 100 μ l of Celltiter-Glo reagent were added to each well. For the inducible cell lines, staining was performed at Day 8. Luminescence was measured after 10 min with a microplate reader.

The apoptosis assay was performed in nontreated, white-walled flat bottom 96-well plates with the Caspase-Glo 3/7 Assay (Promega, Madison, WI). A single cell suspension of 100 μ l containing 20,000 cells was added to each well. Each plate contained three wells per shRNA-construct, at least three wells with untreated cells and three wells of medium for background measurement. On Day 4, 100 μ l of Caspase-Glo 3/7 reagent was added to each well. Luminescence was measured after 30 min with a microplate reader.

For the comet assay, a total of 2×10^5 cells per condition in three replicates was treated as indicated and embedded in low-melt agarose and spotted on glass slides using the OxiSelect kit (STA-350, Biocat, Heidelberg, Germany). Gel electrophoresis and staining were done according to the manufacturer's protocol. Image was taken with an Olympus ScanR microscope and the analysis was conducted using ImageJ.

FACS analysis

FACS measurements were conducted with a FACSCanto II (BD Biosciences, Heidelberg, Germany) flow cytometer and data

processing and analysis was done with WEASEL 3.2 flow cytometry software. For viability measurements, cells were harvested and stained with TO-PRO3 in FACS buffer (10 mM HEPES, 2.5 mM CaCl₂, 140 mM NaCl) and a FACS analysis was performed 30 min after harvesting. The annexinV/7-AAD staining was conducted on 6-well plates in triplicates by seeding 200,000 separated cells in 1 ml medium per well. Twenty-four hours after shRNA transduction, an additional ml of medium was added to each well. On Day 7, the cells were dissociated, incubated in a buffer containing 10% annexin V and 10% 7-AAD (BD Biosciences) and analyzed by FACS. For the inducible cell lines, this step was performed at Day 9. CD133 staining was performed in 96-well plates in triplicates by seeding a suspension of 15,000 cells in 100 μ l per well. After 24 hr, 100 μ l of fresh medium was added. On Day 5, the cells were dissociated, stained with a PE conjugated CD133/1 antibody (clone AC133, Miltenyi Biotec, Bergisch Gladbach, Germany) and subjected to FACS analysis. For the inducible cell lines, this step was performed at Day 9. The propidium iodide staining was performed in 96-well plates in triplicates with a suspension of 15,000 cells in 100 μ l per well. After 24 hr, 100 μ l of fresh medium was added. On Day 6, the cells were dissociated, stained with propidium iodide (Sigma, Munich, Germany) and analyzed by FACS.

Data availability

All original sequencing data have been deposited at the European Genome-phenome Archive (EGA, <http://www.ebi.ac.uk/ega/>) under the accession number EGAS00001003750. The processed sequencing data are available at the Gene Expression Omnibus (GEO, <https://www.ncbi.nlm.nih.gov/geo/>) database under the accession number GSE122832.

Results

GICs have an open chromatin structure

In previous studies, an open and "hyperdynamic" chromatin conformation has been identified as a general feature of stem cells with chromosomal proteins exchanging more rapidly than in somatic cells.^{11,32,33} mESCs represent a well-established reference system for this type of increased chromatin plasticity in comparison to neural progenitor cells derived from them.^{13,34} Consistent with these previous studies, we found that heterochromatin protein 1 alpha (HP1 α) as well as the histone methylase SUV39H1 that sets the H3K9me3 mark displayed increased dynamics in their chromatin interactions in mESCs (Supplementary Fig. S1). Next, we tested whether these stem cell chromatin features were also present in GICs and corresponding controls (Fig. 1 and Supplementary Table S2). Undifferentiated human adult neuronal stem cells from the subventricular zone (SVZ-NPC) showed a homogenous distribution of HP1 α and the H3K9me3 modification and both features accumulated into distinct nuclear foci upon differentiation with retinoic acid (Fig. 1a). We then compared the GIC cell line NCH421k with retinoic acid differentiated NCH421k (NCH421k-diff) cells²⁹ (Fig. 1b). NCH421k cells displayed the same disperse distribution of heterochromatin

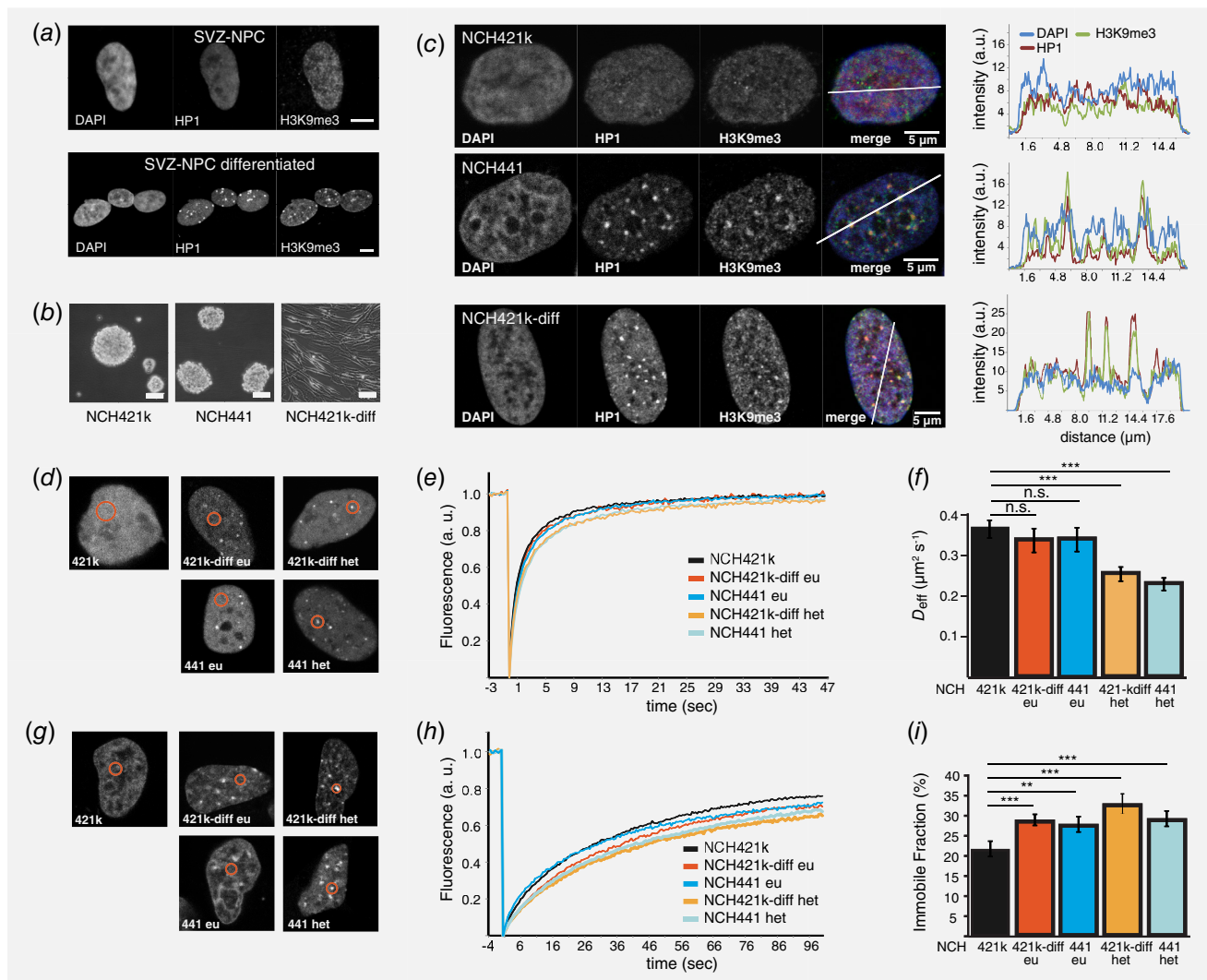


Figure 1. Differences in morphology and chromatin organization of cell types studied. (a) Immunofluorescence of HP1 α and H3K9me3 in human adult neuronal precursor cells (SVZ-NPC) before (top row) and after differentiation (bottom row). Scale bar 5 μ m. (b) Morphology of cell lines studied by light microscopy. Both NCH421k and NCH441 grew in neurospheres and proliferated but NCH441 has low tumor initiation potential. NCH421k-diff cells were derived from NCH421k by inducing differentiation with retinoic acid, which results in adherently growing cells. Scale bar 50 μ m. (c) Fluorescence microscopy images of the distribution of HP1 α and H3K9me3 in NCH421k, NCH441 and NCH421k-diff. HP1 α and H3K9me3 showed foci formation in differentiated cells and in the NCH441 cell line. In NCH421k cells, both heterochromatin markers were more homogeneously distributed. This topology is reflected in the intensity profile plots along the white line through the nucleus. Scale bar 5 μ m. (d) Examples of HP1 α bleached regions in the three different cell types. (e) Averaged FRAP curves from at least 30 measurements. Two curves for eu- and heterochromatin are shown for both NCH441 and NCH421k-diff cells, while the unstructured NCH421k chromatin is represented by a single curve. (f) Differences in mobility were quantitated from an effective diffusion coefficient obtained by fitting individual FRAP curves. Lower diffusion coefficients were measured for HP1 α in dense regions of both NCH441 and NCH421k-diff cells as HP1 α recovered slower than in NCH421k. The error bars represent the SEM; *** p < 0.001. (g) Same as in panel (d) but for SUV39H1. (h) Same as in panel (e) but for SUV39H1. (i) For SUV39H1, a binding model described the recovery curves well. The resulting kinetic dissociation rate constant was similar with $k_{off} \sim 0.04$ /sec. Significantly more immobile SUV39H1 was present NCH441 and NCH421k-diff cells than in NCH421k as shown in the plot. The error bars represent the SEM; *** p < 0.001; ** p < 0.01. [Color figure can be viewed at wileyonlinelibrary.com]

markers throughout the nucleus with a morphology very similar to the neuronal stem cells (Fig. 1c, top and Fig. 1a). In contrast, dense heterochromatin foci were detected in NCH421k-diff cells (Fig. 1c, bottom). To exclude indirect effects of retinoic acid on chromatin organization, we included a CD133 negative cell line NCH441 as a reference (Fig. 1b). In contrast to NCH421k, NCH441 has low tumorigenic potential as shown

in mouse xenograft experiments (Supplementary Table S3). Consistent with the proposed relation between global chromatin features and the self-renewal potential, we observed distinct heterochromatin foci in NCH441 (Fig. 1c, middle). Eight, seven and one foci were counted on average for NCH421k-diff, NCH441 and NCH421k, respectively (Supplementary Fig. S2a), and global H3K9me3 levels increased upon differentiation

(Supplementary Fig. S2*b*). The heterochromatin foci were also present in FACS-sorted CD133 negative NCH644 cells but not in CD133 positive cells, which would represent the GIC fraction in this cell line (Supplementary Fig. S2*c*). Using IF, we quantified levels of histone acetylation and H3K4me3 as markers for open chromatin. Both histone acetylation and H3K4me3 were elevated in NCH421k as compared to the CD133 negative NCH441 clone (Supplementary Fig. S2*d*).

Next, we evaluated whether the globally decondensed chromatin structure in NCH421k correlated with a faster exchange of chromatin-bound HP1 α and SUV39H1 in comparison to NCH421k-diff and NCH441. A quantitative FRAP analysis was conducted as described previously for these two proteins.^{31,35} We found that both HP1 α and SUV39H1 were significantly more mobile in the NCH421k GIC cell line (Figs. 1*d–i* and Supplementary Table S1). In NCH421k cells, HP1 α showed a recovery rate that was comparable with NCH441 and NCH421k-diff cells for euchromatin as quantitated by the effective diffusion coefficient (Figs. 1*e* and 1*f*). The difference in mobility became more pronounced when heterochromatic regions were included, demonstrating that HP1 α binds more tightly at nuclear

subcompartments where it is enriched. The immobile fraction comprised only 1–2% and was similar in all cell types and chromatin subcompartments. In contrast, for SUV39H1 the immobile fraction (average residence time >2 min in the chromatin bound state) was reduced by about 10% in NCH421k GICs as compared to the other cell types (Figs. 1*h* and 1*i*). Thus, high affinity sites of SUV39H1 protein as represented by its immobile fraction were considerably more abundant in differentiated cells. From a fit of the data to a binding model, a kinetic dissociation rate of $k_{\text{off}} = 0.04/\text{sec}$ and a lifetime of $1/k_{\text{off}} = 25 \text{ sec}$ for the mobile SUV39H1 fraction was obtained for all cell types suggesting that the corresponding binding sites are present in all cell types.

In summary, we conclude that GICs have a stem cell-like, globally decondensed and more dynamic chromatin organization in comparison to their non-tumorigenic counterparts. The global chromatin state was characterized by the absence of foci that contained HP1 α , SUV39H1 and H3K9me3 and elevated histone acetylation levels. HP1 α and SUV39H1 displayed reduced chromatin-binding affinity to chromatin as compared to the non-tumorigenic reference cell types.

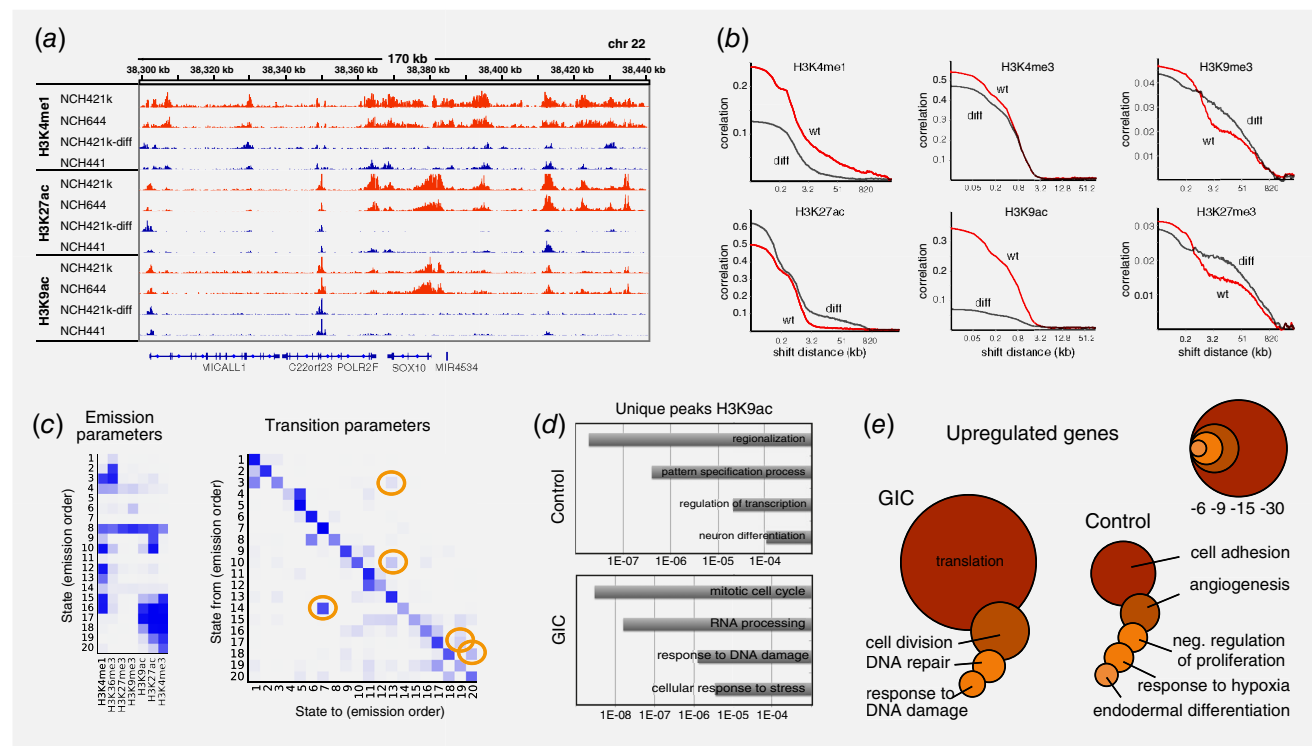


Figure 2. ChIP-seq and RNA-seq analysis of GIC differentiation. The NCH421k and NCH644 GIC cell lines were compared to differentiated NCH421k-diff and NCH441 that lack glioblastoma initiating capacity. (a) Exemplary traces of histone modifications from ChIP-seq around the SOX10 locus are depicted. Promoter and enhancer acetylation at this locus were only present in GICs. (b) Correlation function analysis of histone modifications throughout the genome. The H3K9ac modification was lost while heterochromatic H3K9me3 and H3K27me3 domain in the range of 3–50 kb were gained during differentiation. (c) ChromHMM analysis of GICs and differentiated GICs. The orange circles mark pronounced changes in states during differentiation. These mostly occurred in states that included H3K4me1, H3K27ac and H3K9ac in the undifferentiated cells. (d) GO analysis of H3K9ac enriched regions identified from peak calling of the ChIP-seq data. (e) Annotation of differentially expressed genes. GO terms enriched for upregulated genes in GICs and differentiated GICs are depicted. The size of circles represents the log *p*-value calculated from the GO analysis. [Color figure can be viewed at wileyonlinelibrary.com]

GICs display H3K9ac enrichment and loss of H3K9me3 and H3K27me3

To identify deregulated histone lysine modifications in GICs, we mapped H3K4me1, H3K4me3, H3K9ac, H3K9me3, H3K27ac, H3K27me3 and H3K36me3 by ChIP-seq in NCH421k and NCH644 GIC cells vs. differentiated NCH421k and NCH441 cells as controls (Fig. 2a). To compare the extension and abundance of domains with different histone modifications, we calculated their correlation functions as described previously³⁶ (Fig. 2b). For both H3K4me1 and H3K9ac, much higher amplitudes were observed for GICs indicative of an enrichment of these marks at specific loci in the undifferentiated state. Both heterochromatic H3K9me3 and H3K27me3 marks displayed an increase of larger domains in the range of 3–50 kb in differentiated cells. The ChromHMM state annotation derived from the histone mark distribution showed that regions enriched for both H3K4me1 and H3K27ac or H3K4me1 alone changed upon differentiation to H3K4me1 only or to an unmodified state, respectively (Fig. 2c). This suggests that active enhancers were reverted to their poised state during differentiation and that poised enhancers were rendered inactive. Additionally, nearly all regions that harbored H3K9ac in GICs retained a lower signal for this mark upon differentiation (Supplementary Fig. S3a). These

results were fully consistent with the findings from the microscopy image analysis and indicate that H3K9me3 and H3K27me3 formed large domains (>50 kb) upon differentiation, whereas H3K9ac was generally enriched in GICs.

Next, we investigated H3K9ac at promoters and enhancers as identified by the presence of H3K4me1 and H3K27ac. Overall, our analysis shows that GIC-specific H3K9ac genes were enriched in the functional GO cluster of cell cycle and response to DNA damage (Fig. 2d). Unique active enhancers were linked to genes involved in the Wnt signaling cascade and cell fate processes (Supplementary Fig. S3b). H3K9ac in the control cells was enriched in genes associated with regionalization, neuronal development and differentiation (Fig. 2d). These findings were also reflected in the RNA-seq analysis. Upregulated genes in GICs were related to cell cycle and response to DNA damage, whereas cell adhesion and differentiation were among the top enriched GO terms for differentiated GICs (Fig. 2e).

From the peak calling analysis of the ChIP-seq data, promoters were identified that had H3K9ac only in GICs. These promoters represent potential target sites for histone demethylases in GICs, since differential histone demethylation activity could lead to a loss of H3K9 methylation and subsequent acetylation of demethylated H3K9.

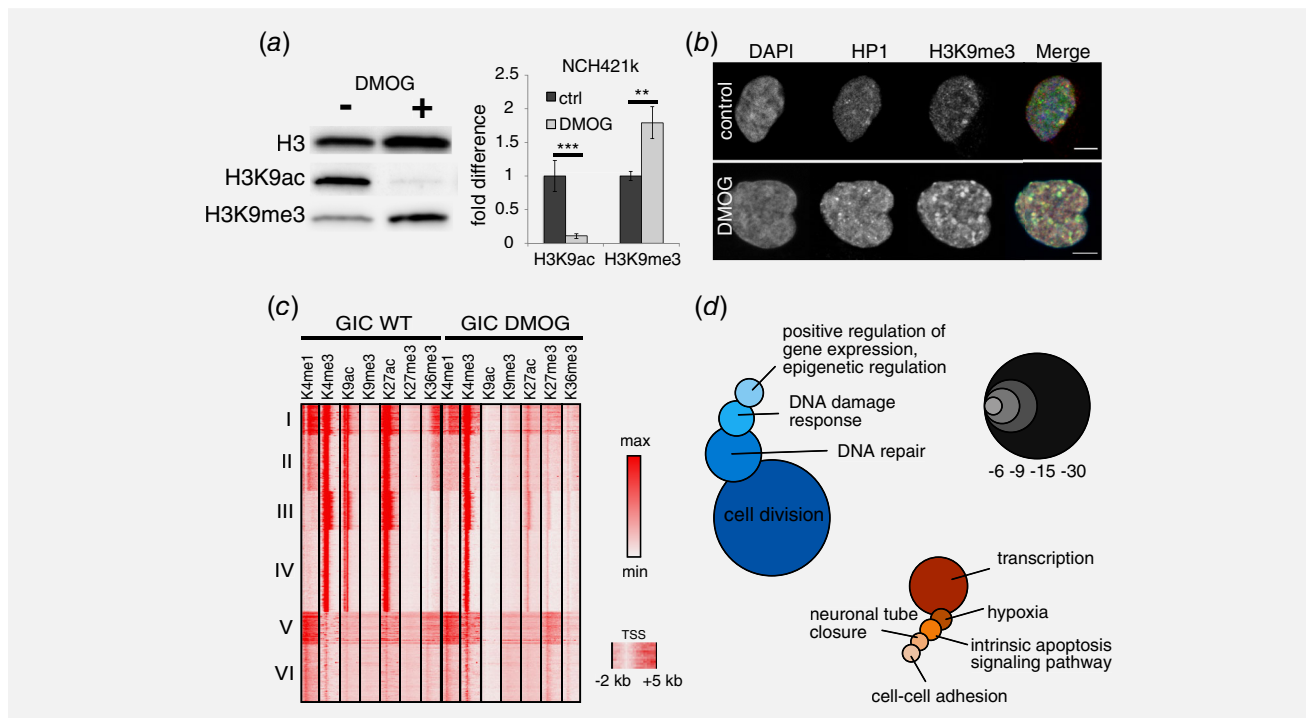


Figure 3. DMOG-induced changes of the histone modifications. (a) Western blot of DMOG-treated NCH421k cells. The bar plot shows its quantification from three replicates. A 1.8-fold increase in H3K9me3 and loss of H3K9ac was measured after normalizing the signal to H3. Error bars indicate the standard deviation (***) $p < 0.001$; ** $p < 0.01$ from t test). (b) IF of HP1 and H3K9me3 after DMOG treatment. DMOG-induced heterochromatin foci formation appeared as bright HP1 and H3K9me3 clusters. Scale bar 5 μ m. (c) Heatmap of genome-wide histone modification pattern at GIC NCH421k promoters. Each line corresponds to one promoter. The different modification signatures fell into the indicated six clusters. Both H3K9ac and H3K27ac marks were largely reduced upon DMOG treatment. (d) Enriched GO terms for upregulated and downregulated genes (red and blue circles, respectively) after DMOG-treatment derived from a differential expression analysis. The size of circles represents the log p -value calculated from the GO analysis. [Color figure can be viewed at wileyonlinelibrary.com]

DMOG treatment increases the H3K9me3-H3K9ac ratio in GICs

Our findings suggest that inhibiting histone demethylation activity could change the histone modification patterns of GICs toward the differentiated state. To test this hypothesis, we employed DMOG as a broad range lysine-demethylase inhibitor.³⁷ Two days of inhibition with DMOG led to twofold higher H3K9me3 levels in NCH421k cells and loss of H3K9ac (Fig. 3a). In addition, DMOG treatment induced heterochromatin foci (Fig. 3b), while transfection of NCH421k-diff cells with the histone demethylase KDM4C reduced heterochromatic H3K9me3 foci and released HP1 α from these sites (Supplementary Fig. S4). Overexpression of KDM4C in differentiated GICs did not induce any detectable

changes in morphology or proliferation within the observed time frame of 72 hr.

To further dissect the DMOG-induced chromatin reorganization, we prepared ChIP-seq and RNA-seq libraries for untreated and 48 hr DMOG-treated cells and followed both the changes in histone modifications and gene expression. In line with the western blot analysis, the resulting ChIP-seq profiles revealed a strong DMOG-induced reduction of histone acetylation marks at promoters for GICs (Fig. 3c), while this effect was only moderate for differentiated GICs. In addition to the global enrichment of H3K9me3, we found a TSS-associated enrichment of H3K27me3 after DMOG treatment (Fig. 3c). This transition was accompanied by a reduction and partial relocation of the H3K36me3

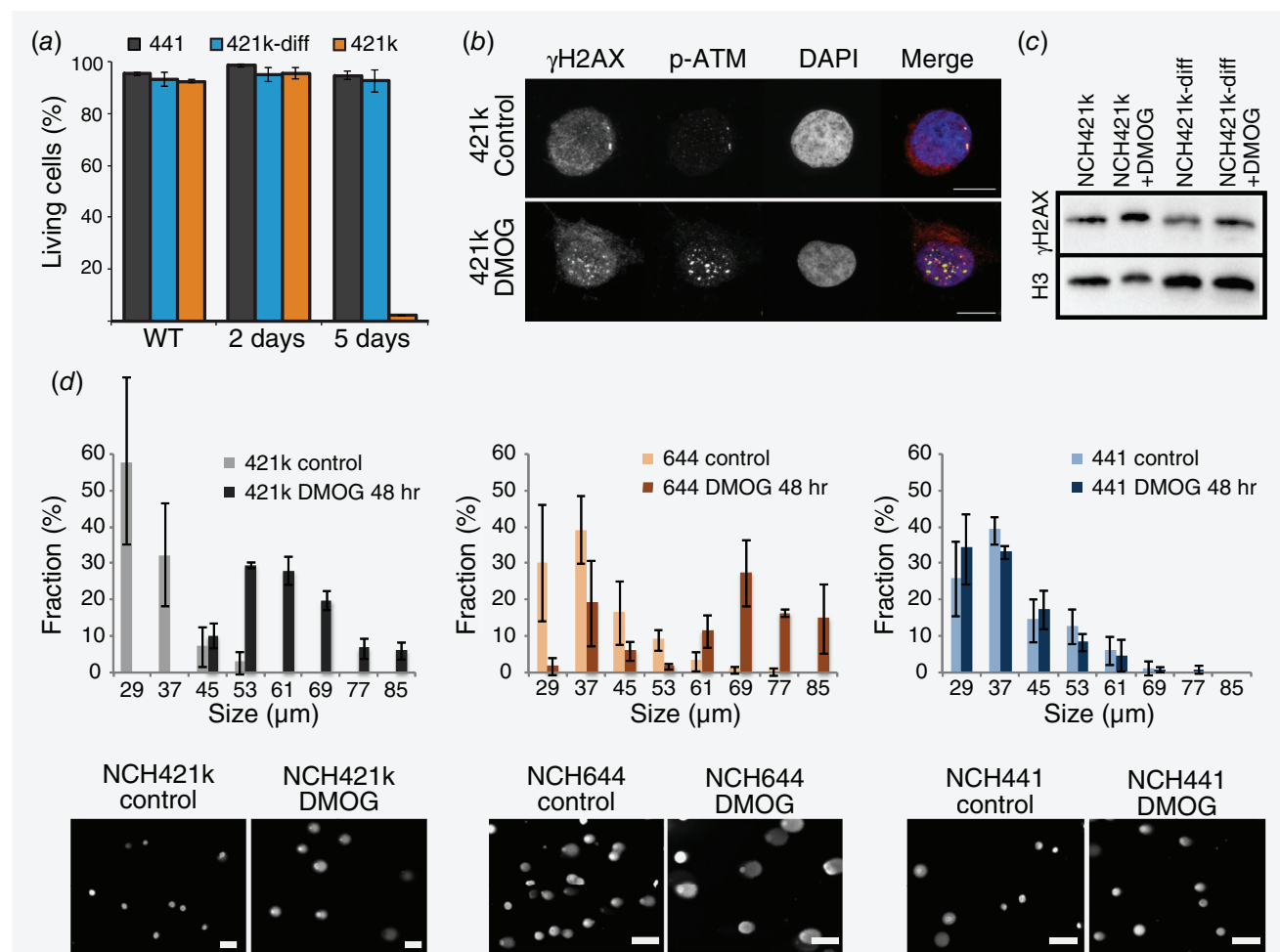


Figure 4. DMOG-induced effects on GIC viability and DNA damage. (a) FACS analysis of DMOG-induced apoptosis measured by TO-PRO3 uptake. The fraction of living cells is plotted. After 5 days, essentially all DMOG-treated NCH421k cells had died while differentiated cells were unaffected. (b) IF of γ H2A.X after 2 days of DMOG treatment showing a large increase in the number of DNA damage foci. (c) Western blot after 48 hr DMOG treatment. An increase in global γ H2A.X phosphorylation levels in NCH421k but not in differentiated NCH421k cells was observed. (d) Histogram of comet size distribution as measured by microscopy for DMOG-treated vs. untreated cells from three replicates. Change in the size distribution was not significant for the NCH441 cell line but highly significant for both NCH421k and NCH644 (p -value below 0.0001). Error bars represent the standard deviation. Microscopy pictures showing representative cells from the comet assay are depicted at the bottom. The analysis shows the accumulation of DNA breaks after DMOG treatment in both GIC cell lines but not in the control NCH441 cell line. Scale bar 100 μ m. [Color figure can be viewed at wileyonlinelibrary.com]

signal to the TSS suggesting a reduced transcriptional (elongation) activity at corresponding genes. The change of H3K36me3 was not observed in differentiated glioblastoma cells, while H3K9me3 and H3K27me3 levels were moderately increased globally (Supplementary Fig. S3a). Both H3K4me1 and H3K4me3 were unaffected by DMOG treatment in both cell types (Fig. 3c and Supplementary Fig. S3a).

Functional clustering analysis of differentially expressed genes after DMOG treatment revealed DNA repair and cell cycle as the main targets (Fig. 3d and Supplementary Tables S6 and S7). A quarter of genes downregulated after DMOG treatment overlapped with those that were primarily marked by H3K9ac at their promoters. DMOG induced genes of the MAPK, HIF1 and Notch pathways (Supplementary Table S6).³⁸ Overall, genes downregulated by DMOG and genes upregulated in GICs in comparison to GIC-diff cells were enriched in the same pathways.

DMOG treatment enhances the DNA damage susceptibility of GICs

To assess the functional relevance of the DMOG-induced changes, we evaluated the cell viability. Cells were treated with DMOG at a concentration of 2.5 mM for 2 and 5 days. At these time points, cells were harvested and stained with TO-PRO3 to identify apoptotic cells that incorporated this dye. After 5 days of

treatment, the vast majority of NCH421k cells became apoptotic, while the other cell types were largely unaffected (Fig. 4a). The DMOG treatment increased the level of the DNA damage marker γ H2A.X as shown by IF and western blot already after 2 days (Figs. 4b and 4c). The DMOG-treated cells displayed an increase in γ H2A.X foci that colocalized with phosphorylated ATM, which is the active form of the central signaling kinase in the DNA double-strand break repair pathway (Fig. 4b). To confirm that the above markers indeed reflected an accumulation of DNA double strand breaks, we analyzed cells 48 hr after DMOG treatment with the comet assay. As depicted in Figure 4d, DNA damage accumulated as apparent from the characteristic “comet tail” structures in both GIC cell lines but not in the control cell line (*p*-values below 0.0001 for both NCH421k and NCH644 and above 0.2 for NCH441). We conclude from the above experiments that histone demethylation activity is important for DNA damage repair and viability GICs.

KDM4C and KDM7A histone demethylases are essential to maintain GIC viability

As DMOG affects also non-KDM targets, we performed an shRNA analysis to validate the importance of specific histone demethylases for the deregulated chromatin state of GICs. To this end, we established stable cell lines of NCH644 GICs to conduct an

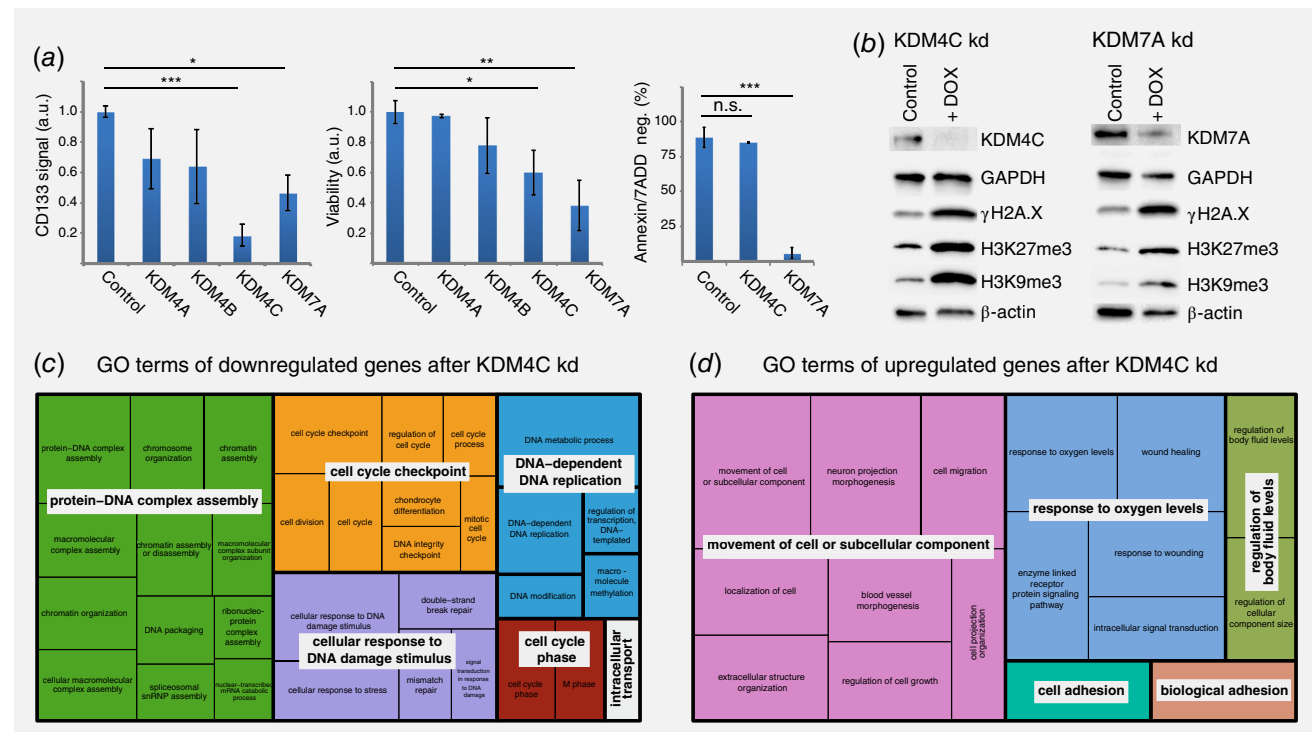


Figure 5. Knockdown of KDM4C and KDM7A histone demethylases. (a) FACS analysis after shRNA induction. The knockdown of KDM4C and KDM7A led to a loss of CD133 in NCH644 GICs as compared to nontarget (NT) controls and reduced viability. An accumulation of apoptotic cells (small fraction of Annexin/7ADD negative cells) was apparent upon KDM7A depletion. All values were normalized to nontarget control. ****p* < 0.001; ***p* < 0.01; **p* < 0.05. (b) Western blot after shRNA induction. For both KDM4C and KDM7A, the knockdown was efficient. H3K9me3 and H3K27me3 levels increased upon knockdown as well as γ H2A.X indicating accumulation of DNA damage. (c) Revigo plot of GO terms of genes downregulated after knockdown of KDM4C. (d) Same as in panel (c) for upregulated genes. [Color figure can be viewed at wileyonlinelibrary.com]

inducible knockdown of H3K9me2/3 and H3K36me2/3 demethylases KDM4A (JMJD2A), KDM4B (JMJD2B) and KDM4C (JMJD2C) as well as KDM7A (JHDM1D) that demethylates H3K9me1/2 and H3K27me1/2.³⁹ Each KDM was knocked down with two shRNA constructs, and cell viability was measured by a luminescence assay. In addition, a FACS analysis was conducted to assess apoptosis *via* Annexin/7-AAD staining and stemness/differentiation with the CD133 marker. The siRNAs targeting of KDM4C induced differentiation as evident by the loss of CD133 while KDM7A knockdown resulted in apoptosis (Fig. 5a). In contrast, knockdown of KDM4A and KDM4B was not associated with a differentiation or apoptosis phenotype. Furthermore, the depletion of KDM4C and KDM7A increased H3K9me3 and H3K27me3 levels and the DNA damage γ H2A.X phosphorylation marker (Fig. 5b).

Next, for KDM4C and KDM7A, RNA-seq libraries of induced and uninduced cells for two different shRNAs per target were prepared. Differential expression analysis for KDM7A revealed only a small number of downregulated and upregulated genes which were associated with fundamental metabolic processes and regulation of neuronal differentiation, respectively (Supplementary Tables S8 and S9). This is in line with the finding that both viability and stemness were impaired after knockdown as shown by our FACS assays. Knockdown of KDM4C resulted in downregulation of a set of genes involved in DNA repair that was similar to the genes with exclusive H3K9ac at their promoters and reflects a loss of proliferation capacity (Fig. 5c). This finding corroborates the conclusion that H3K9ac promoters are indeed KDM targets. The differentiation phenotype that was observed after KDM4C knockdown can be rationalized by the activation of genes involved in neuron projection morphogenesis, adhesion and response to oxygen levels after knockdown—all pathways that were upregulated after differentiation or treatment with DMOG (Fig. 5d). The results demonstrate that KDM4C and KDM7A are crucial for DNA repair and genome integrity and thus survival of GICs.

Discussion

The frequent tumor relapse during treatment of glioblastoma might originate from a small subpopulation of GICs with stem cell characteristics such as multipotency and self-renewal.^{5,6} Accordingly, exploiting the stem cell-like chromatin features of these cells as drug targets could represent a novel approach to develop more efficient treatment strategies. Here, we report on the deregulated epigenetic network in GICs that is centered around H3K9me2/3. In these cells, the latter mark was depleted at promoters while the opposing H3K9ac modification was strongly enriched. In addition, we found GIC-specific activities of the H3K9me2/3 reader protein HP1 α as well methyltransferases like SUV39H1 and the JMJ-type demethylases KDM4C and KDM7A that can remove these marks. Another repressive mark, H3K27me3, displayed a reduced domain size in GICs, which supports the conclusion that chromatin in these cells is in a more open and plastic stem cell-like state. Furthermore, it is noted that deregulation of H3K27me3 was recently linked to the presence of bivalent chromatin domains in

glioblastoma subtypes that pointed toward dedifferentiation into a more stem cell-like phenotype.⁴⁰

Since KDM enzymes can be competitively inhibited with α -ketoglutarate mimics like DMOG,^{37,41} we evaluated the cellular response toward this compound. Remarkably, inhibition of NCH421k and NCH644 GICs with DMOG restored global H3K9me3 levels to that of the differentiated references, led to DNA damage and induced cell death specifically in the GIC cell lines. In contrast, the non-tumorigenic controls as well as differentiated cycling and non-cycling cells were not affected. Neither DNA damage nor apoptosis was induced in the controls as shown by γ H2A.X levels and the comet assay. Thus, we conclude that inhibition of histone demethylases that use α -ketoglutarate as a donor has little impact on differentiated cells.

The gene expression changes underlying the selective killing of GICs by DMOG were dissected by RNA-seq. About 75% of DMOG-responsive genes were downregulated and showed loss of H3K9 acetylation promoter peaks present in untreated GICs that were enriched at DDR genes. Thus, constant histone demethylation was needed for lysine acetylation at these promoters. DMOG is also a potent stabilizer of hypoxia inducible factor 1 (HIF-1) that inhibits differentiation by inducing the Notch signaling pathway,⁴² which could promote self-renewal and survival of GICs.^{43,44} Indeed, Notch target genes were induced upon DMOG treatment as inferred from the RNA-seq analysis. However, the potential effects of Notch induction appeared to be secondary to the loss of viability due to repression of DNA repair pathways.

KDMs have previously been reported to play a central role in tumor growth, proliferation and survival.^{45–49} In our study, the knockdown of several KDMs revealed that the histone demethylases KDM4C and KDM7A acting on H3K9me2/me3 were essential to maintain GICs. Interestingly, our RNA-seq data did not reveal an overexpression of KDM4C or KDM7A transcripts in GICs. This suggests that the deregulated activity of these KDMs in GICs as compared to differentiated cells occurred either on the protein level or was related to different gene targeting modes. We found that KDM4C knockdown mainly affected genes involved in DNA repair with a phenotype that was similar to DMOG treatment. It is noted that efficient DDR is a key characteristic of both normal and cancer stem cells and essential for their resistant to DNA damaging drugs.⁵⁰ KDM4 enzymes contribute to this activity and overexpression of KDM4B was linked to a higher efficiency of DDR after irradiation.⁵¹ Furthermore, it has been shown that the self-renewal capacity of ESCs requires KDM4B and KDM4C to prevent accumulation of H3K9me3 at promoters⁵² while the H3K9me3 mark blocks reprogramming into induced pluripotent stem cells.^{17,18} Thus, the reduction of H3K9me3 *via* an increased KDM4 activity and the concomitant rise of H3K9ac levels appears to be a crucial chromatin feature of the stem cell state that is reproduced in the GIC cell lines studied here. KDM7A, the other demethylase we found as essential for GIC viability, appears to have different targets. Its knockdown repressed vital metabolic genes. Interestingly, for both KDMs genes

upregulated upon knockdown were mainly associated with activities linked to differentiation.

We conclude that KDM4C and KDM7A represent promising drug targets for GICs by inducing differentiation and apoptosis. Since their activity was linked here to maintenance of a deregulated DDR, we predict that the effect of KDM inhibition can be further enhanced by a combination with DNA damage inducing agents. It is noted that KDM4 inhibition was recently shown to target stem-like cells also in breast

cancer⁵³ raising the possibility that increased KDM4 activity is a general feature of tumor inducing cells.

Acknowledgements

This work was funded by the Cooperation Program in Cancer Research of the German Cancer Research Center (DKFZ) and Israel's Ministry of Science, Technology and Space (MOST) via grants Ca146 and Ca180 to K.R. and E.M. J.P.M. was supported by the German CellNetworks Cluster of Excellence (EXC81) and RG and CHM by the Anni Hofmann foundation.

References

- Holland EC. Glioblastoma multiforme: the terminator. *Proc Natl Acad Sci U S A* 2000;97:6242–4.
- Dean M. Cancer stem cells: redefining the paradigm of cancer treatment strategies. *Mol Interv* 2006;6:140–8.
- Reya T, Morrison SJ, Clarke MF, et al. Stem cells, cancer, and cancer stem cells. *Nature* 2001;414:105–11.
- Singh SK, Hawkins C, Clarke ID, et al. Identification of human brain tumour initiating cells. *Nature* 2004;432:396–401.
- Gil J, Stembalska A, Pesz KA, et al. Cancer stem cells: the theory and perspectives in cancer therapy. *J Appl Genet* 2008;49:193–9.
- Zhou J, Zhang Y. Cancer stem cells: models, mechanisms and implications for improved treatment. *Cell Cycle* 2008;7:1360–70.
- Bao S, Wu Q, McLendon RE, et al. Glioma stem cells promote radioresistance by preferential activation of the DNA damage response. *Nature* 2006;444:756–60.
- Eramo A, Ricci-Vitiani L, Zeuner A, et al. Chemotherapy resistance of glioblastoma stem cells. *Cell Death Differ* 2006;13:1238–41.
- Tamura K, Aoyagi M, Wakimoto H, et al. Accumulation of CD133-positive glioma cells after high-dose irradiation by gamma knife surgery plus external beam radiation. *J Neurosurg* 2010;113:310–8.
- Meshorer E, Misteli T. Chromatin in pluripotent embryonic stem cells and differentiation. *Nat Rev Mol Cell Biol* 2006;7:540–6.
- Schlesinger S, Meshorer E. Open chromatin, epigenetic plasticity, and nuclear organization in pluripotency. *Dev Cell* 2019;48:135–50.
- Arney KL, Fisher AG. Epigenetic aspects of differentiation. *J Cell Sci* 2004;117:4355–63.
- Meshorer E, Yellajoshula D, George E, et al. Hyperdynamic plasticity of chromatin proteins in pluripotent embryonic stem cells. *Dev Cell* 2006;10:105–16.
- Mikkelsen TS, Ku M, Jaffe DB, et al. Genome-wide maps of chromatin state in pluripotent and lineage-committed cells. *Nature* 2007;448:553–60.
- Niwa H. Open conformation chromatin and pluripotency. *Genes Dev* 2007;21:2671–6.
- Krejci J, Uhlířová R, Galiová G, et al. Genome-wide reduction in H3K9 acetylation during human embryonic stem cell differentiation. *J Cell Physiol* 2009;219:677–87.
- Soufi A, Donahue G, Zaret KS. Facilitators and impediments of the pluripotency reprogramming factors' initial engagement with the genome. *Cell* 2012;151:994–1004.
- Chen J, Liu H, Liu J, et al. H3K9 methylation is a barrier during somatic cell reprogramming into iPSCs. *Nat Genet* 2013;45:34–42.
- Hezroni H, Tzchori I, Davidi A, et al. H3K9 histone acetylation predicts pluripotency and reprogramming capacity of ES cells. *Nucleus* 2011;2:300–9.
- Loh YH, Zhang W, Chen X, et al. Jmjd1a and Jmjd2c histone H3 Lys 9 demethylases regulate self-renewal in embryonic stem cells. *Genes Dev* 2007;21:2545–57.
- Toiber D, Erdel F, Bouazoune K, et al. SIRT6 recruits SNF2H to DNA break sites, preventing genomic instability through chromatin remodeling. *Mol Cell* 2013;51:454–68.
- Nakamura K, Kato A, Kobayashi J, et al. Regulation of homologous recombination by RNF20-dependent H2B ubiquitination. *Mol Cell* 2011;41:515–28.
- Murr R, Loizou JI, Yang YG, et al. Histone acetylation by Trapp-Tip60 modulates loading of repair proteins and repair of DNA double-strand breaks. *Nat Cell Biol* 2006;8:91–9.
- Goodarzi AA, Jeggo PA. The heterochromatic barrier to DNA double strand break repair: how to get the entry visa. *Int J Mol Sci* 2012;13:11844–60.
- Chiolo I, Minoda A, Colmenares SU, et al. Double-strand breaks in heterochromatin move outside of a dynamic HP1a domain to complete recombinational repair. *Cell* 2011;144:732–44.
- Torres CM, Biran A, Burney MJ, et al. The linker histone H1.0 generates epigenetic and functional intratumor heterogeneity. *Science* 2016;353:aaf1644.
- Mallm JP, Tschape JA, Hick M, et al. Generation of conditional null alleles for APP and APLP2. *Genesis* 2010;48:200–6.
- Ernst A, Hofmann S, Ahmadi R, et al. Genomic and expression profiling of glioblastoma stem cell-like spheroid cultures identifies novel tumor-relevant genes associated with survival. *Clin Cancer Res* 2009;15:6541–50.
- Campos B, Wan F, Farhadi M, et al. Differentiation therapy exerts antitumor effects on stem-like glioma cells. *Clin Cancer Res* 2010;16:2715–28.
- Campos B, Gal Z, Baader A, et al. Aberrant self-renewal and quiescence contribute to the aggressiveness of glioblastoma. *J Pathol* 2014;234:23–33.
- Muller KP, Erdel F, Caudron-Herger M, et al. Multiscale analysis of dynamics and interactions of heterochromatin protein 1 by fluorescence fluctuation microscopy. *Biophys J* 2009;97:2876–85.
- Melcer S, Hezroni H, Rand E, et al. Histone modifications and Lamin A regulate chromatin protein dynamics in early embryonic stem cell differentiation. *Nat Commun* 2012;3:910.
- Bhattacharya D, Talwar S, Mazumder A, et al. Spatio-temporal plasticity in chromatin organization in mouse cell differentiation and during Drosophila embryogenesis. *Biophys J* 2009;96:3832–9.
- Mattout A, Aaronson Y, Sailaja BS, et al. Heterochromatin protein 1beta (HP1beta) has distinct functions and distinct nuclear distribution in pluripotent versus differentiated cells. *Genome Biol* 2015;16:213.
- Muller-Ott K, Erdel F, Matveeva A, et al. Specificity, propagation, and memory of pericentric heterochromatin. *Mol Syst Biol* 2014;10:746.
- Molitor J, Mallm JP, Rippe K, et al. Retrieving chromatin patterns from deep sequencing data using correlation functions. *Biophys J* 2017;112:473–90.
- Hamada S, Kim TD, Suzuki T, et al. Synthesis and activity of N-oxalylglycine and its derivatives as Jumonji C-domain-containing histone lysine demethylase inhibitors. *Bioorg Med Chem Lett* 2009;19:2852–5.
- Gao W, Sweeney C, Connolly M, et al. Notch-1 mediates hypoxia-induced angiogenesis in rheumatoid arthritis. *Arthritis Rheum* 2012;64:2104–13.
- Hofffeldt JW, Agger K, Helin K. Histone lysine demethylases as targets for anticancer therapy. *Nat Rev Drug Discov* 2013;12:917–30.
- Hall AW, Battenhouse AM, Shivram H, et al. Bivalent chromatin domains in glioblastoma reveal a subtype-specific signature of glioma stem cells. *Cancer Res* 2018;78:2463–74.
- Labbe RM, Holowatyj A, Yang ZQ. Histone lysine demethylase (KDM) subfamily 4: structures, functions and therapeutic potential. *Am J Transl Res* 2013;6:1–15.
- Gustafsson MV, Zheng X, Pereira T, et al. Hypoxia requires notch signaling to maintain the undifferentiated cell state. *Dev Cell* 2005;9:617–28.
- Hovinga KE, Shimizu F, Wang R, et al. Inhibition of notch signaling in glioblastoma targets cancer stem cells via an endothelial cell intermediate. *Stem Cells* 2010;28:1019–29.
- Qiang L, Wu T, Zhang HW, et al. HIF-1alpha is critical for hypoxia-mediated maintenance of glioblastoma stem cells by activating Notch signaling pathway. *Cell Death Differ* 2012;19:284–94.
- Ishimura A, Terashima M, Kimura H, et al. Jmjd2c histone demethylase enhances the expression of Mdm2 oncogene. *Biochem Biophys Res Commun* 2009;389:366–71.
- Li W, Zhao L, Zang W, et al. Histone demethylase JMJD2B is required for tumor cell proliferation and survival and is overexpressed in gastric

- cancer. *Biochem Biophys Res Commun* 2011;416:372–8.
47. Kim TD, Jin F, Shin S, et al. Histone demethylase JMJD2A drives prostate tumorigenesis through transcription factor ETV1. *J Clin Invest* 2016;126:706–20.
48. Kim TD, Shin S, Berry WL, et al. The JMJD2A demethylase regulates apoptosis and proliferation in colon cancer cells. *J Cell Biochem* 2012;113:1368–76.
49. Krieg AJ, Rankin EB, Chan D, et al. Regulation of the histone demethylase JMJD1A by hypoxia-inducible factor 1 alpha enhances hypoxic gene expression and tumor growth. *Mol Cell Biol* 2010;30:344–53.
50. Mandal PK, Blanpain C, Rossi DJ. DNA damage response in adult stem cells: pathways and consequences. *Nat Rev Mol Cell Biol* 2011;12:198–202.
51. Young LC, McDonald DW, Hendzel MJ. Kdm4b histone demethylase is a DNA damage response protein and confers a survival advantage following gamma-irradiation. *J Biol Chem* 2013;288:21376–88.
52. Pedersen MT, Agger K, Laugesen A, et al. The demethylase JMJD2C localizes to H3K4me3-positive transcription start sites and is dispensable for embryonic development. *Mol Cell Biol* 2014;34:1031–45.
53. Metzger E, Stepputtis SS, Strietz J, et al. KDM4 inhibition targets breast cancer stem-like cells. *Cancer Res* 2017;77:5900–12.